aerospace

MDPI

Article

Quantifying the Environmental Design Trades for a State-of-the-Art Turbofan Engine

Evangelia Maria Thoma *,†, Tomas Grönstedt † and Xin Zhao †

Division of Fluid Dynamics, Department of Mechanics and Maritime Sciences, Chalmers University of Technology, 412 96 Gothenburg, Sweden; tomas.gronstedt@chalmers.se (T.G.); xin.zhao@chalmers.se (X.Z.)

* Correspondence: marily@chalmers.se

† These authors contributed equally to this work.

Received: 17 August 2020; Accepted: 10 October 2020; Published: 13 October 2020

Abstract: Aircraft and engine technology have continuously evolved since their introduction and significant improvement has been made in fuel efficiency, emissions, and noise reduction. One of the major issues that the aviation industry is facing today is pollution around the airports, which has an effect both on human health and on the climate. Although noise emissions do not have a direct impact on climate, variations in departure and arrival procedures influence both CO_2 and non-CO_2 emissions. In addition, design choices made to curb noise might increase CO_2 and vice versa. Thus, multidisciplinary modeling is required for the assessment of these interdependencies for new aircraft and flight procedures. A particular aspect that has received little attention is the quantification of the extent to which early design choices influence the trades of CO_2, NOx, and noise. In this study, a single aisle thrust class turbofan engine is optimized for minimum installed SFC (Specific Fuel Consumption). The installed SFC metric includes the effect of engine nacelle drag and engine weight. Close to optimal cycles are then studied to establish how variation in engine cycle parameters trade with noise certification and LTO (Landing and Take-Off) emissions. It is demonstrated that around the optimum a relatively large variation in cycle parameters is allowed with only a modest effect on the installed SFC metric. This freedom in choosing cycle parameters allows the designer to trade noise and emissions. Around the optimal point of a state-of-the-art single aisle thrust class propulsion system, a 1.7 dB reduction in cumulative noise and a 12% reduction in EINOx could be accomplished with a 0.5% penalty in installed SFC.

Keywords: turbofan engine; ultra-high bypass engine (UHBPR); installation effects; engine cycle design; LTO cycle; NOx emissions; noise emissions; OPR; FPR

1. Introduction

State-of-the-art turbofan engines convert chemical energy to useful propulsive thrust power with an efficiency of around 40%. This represents an immense historical improvement manifesting a reduction in fuel burn with about 75% since the introduction of the Comet 4 aircraft in the early 1960s [1]. While noise and NOx emissions are subject to regulatory limits, the fuel burn reduction achievements have been pushed primarily by the airliners' drive to invest in more fuel and cost efficient aircraft.

Long-term exposure to high levels of aircraft noise is known to have a significant impact on human health, e.g., cardiovascular disease and sleep disturbance [2,3]. Therefore, reduction of aircraft noise has been a major issue leading to ICAO (International Civil Aviation Organization) issuing a series of regulation recommendations. Most recently, this is manifested by the adoption of the ever stringent ICAO Chapter 14 noise standard [4].

Clearly, the interdependency between fuel efficiency and NOx emissions has been recognized for a long time. Even with the first CAEP/1 (Committee on Aviation Environmental Protection) standard adopted in 1981, this interdependency was accounted for by allowing the emission certification levels to be relaxed with increasing overall pressure ratio (OPR).

Previous studies concerning noise reduction focus on trajectory optimization and take-off and landing procedures as presented in [5] and [6]. Some of them examine trades between engine parameters and noise [6,7]. Antoine and Kroo [6] evaluate noise against BPR for a range of noise abatement procedures. Gliebe and Janardan evaluate noise produced from four different engine designs for a large twin-engine civil aircraft. These engines were assumed to have the same core technology but different fan pressure ratio (FPR) and bypass ratio (BPR) [7]. Work on how NOx emissions depend on engine cycle parameters is introduced by Kyprianidis and Dahlquist in [8], where trades between NOx emissions and specific thrust as well as OPR are examined for engines with two different combustor types. Another study that treats both noise and NOx emissions is presented by Cumpsty et al. [9]. In this work, aspects of air travel are considered for improvement and treated either independently or correlated to each other. LTO NOx levels are examined against varying OPR and are compared to existing goals for present and future flights. It is demonstrated that NOx emissions are highly dependent on combustor exit temperature and OPR, and hence are greatly affected by measures for fuel burn reduction such as increasing the OPR. An optimization case is presented, where the objective function consists of the cumulative noise level and fuel-burn with different weighting factors. It is shown that the solution corresponding to the lowest noise levels leads to significantly increased fuel-burn and the most fuel efficient solution yields higher noise levels.

In this work, in-house codes developed for four different aspects of aircraft system modeling are integrated to simulate interdependencies: (1) engine performance and aircraft flight trajectories, (2) engine conceptual design and sizing, (3) noise modeling, and (4) emissions modeling. The focus of the research is to assess how variation in engine cycle parameters for a state-of-the-art engine affects noise and NOx emissions with a minimum effect on the fuel burn. The process starts from the modeling of the engine and aircraft system. Engine components' efficiencies and temperature limits are defined to model a state-of-the-art single aisle thrust class propulsion system, which is an engine cycle with component efficiencies, cooling technology, component weight assumptions attempting to model the Leap-1A engine. With the engine model in place, the aircraft is modeled based on the A321-200 and trajectories are established through the flight dynamic equations for the aircraft. Keeping the aircraft and mission fixed, an optimization case is examined for variation in OPR, FPR, and BPR, leading to different engine designs and operational characteristics. A simplified metric for mission fuel burn, installed SFC, is used to define the optimal cycle. Trades are then studied around this optimum to quantify on the design choices that engine manufactures have to make upon freezing the cycle of a new engine. Around the cycle optimum, fuel burn varies only slowly. The aim of the paper is to quantify the design trades for a state-of-the-art turbofan single aisle thrust class engine, i.e., assess how large reduction in LTO NOx and cumulative noise that the cycle designer can expect without a substantial increase in fuel burn. To the authors' knowledge, this work represents the first study that considers the combined problem of NOx and noise trades around minimum fuel burn point.

2. Materials and Methods

To allow the coupled study of aircraft trajectories, noise, NOx, and CO_2 emissions, a number of simulation modules are linked together within a Python-based framework. At the heart of the simulation, the Chalmers in-house code for aircraft engine simulations, GESTPAN (GEneral Stationary and Transient Propulsion ANalysis), is used [10]. GESTPAN feeds data to the weight and dimensions model WEICO (WEight and COst estimation) [11], the emissions model CHEESE (CHalmers Engine Emissions Simulation Environment), and the noise model CHOICE (CHalmers nOIse CodE, [12]).

2.1. Engine Performance Modeling and Conceptual Design

To analyze the thermodynamic performance of a state-of-the-art turbofan engine, a model was set up for an engine with a take-off thrust (Mach 0.0) of 143 kN. For this purpose, GESTPAN and WEICO were used. GESTPAN is a simulation system for aircraft and propulsion performance that allows the user to perform design, off-design, and transient analysis. It has been used and validated in several projects and studies, such as [13] and [14].

WEICO is a tool that allows for the engine conceptual design and sizing. Its validation is supported by a number of projects such as VITAL [15] and NEWAC [16]. WEICO reads the engine performance data generated by GESTPAN and estimates the weight and geometric characteristics of the engine components for the selected design point. The engine weight and size are then inserted into the aircraft model in GESTPAN, and the fuel consumption is evaluated, accounting for engine installation effects. This system is responsible for the design optimization of the solution. The weight and size calculation are integrated into the optimization procedure and vary for every new engine evaluated.

The installed drag includes not only conventional installation effects such as engine bleed and power extraction but also the detrimental effect of nacelle drag and added drag due to carrying the weight of the engine:

$$SFC_{installed} = b/(F_N - D_{engine\ mass} - D_{nacelle}) \quad (1)$$

The basic expression used to establish the optimal engine is included in Equation (1) above as evaluated in the cruise point. The nacelle drag term is calculated using Equation (2):

$$D_{nacelle} = C_{d\_nac}\ A_{max}\ q \quad (2)$$

where C_{d_nac} is the total nacelle drag coefficient, which is calculated as the summation of the pressure drag coefficient, the skin friction drag coefficient, and the spillage drag coefficient as introduced in the ESDU report [17]. The value of the coefficient varies with the fan diameter and ranges from 0.022 to 0.024, which is within the limits found in public literature [17,18] for conventional nacelle design of an ultra-high bypass ratio engine. The concept of installed SFC is generally more complicated than simply accounting for the nacelle drag, as it is also affected by engine positioning, pylon design, etc. However, this is the most important factor and is believed to be sufficient for the preliminary studies presented in this work.

Engine parameters were chosen based on data found in [19] and the ICAO Emissions Databank [20]. However, limited engine performance data are publicly available for the given engine. Thus, component efficiencies are based on trending performance parameters [21] and trends developed based on research data as presented in [22]. Following the methodology described in [22], GESTPAN and WEICO were put together to establish engine component efficiencies based on the year of entry into service, the component size, and the Reynolds number. At top-of-climb, a temperature of 1650 K was assumed for the turbine inlet temperature and a pressure ratio split exponent of 0.25. Top-of-climb key design data together with thrust requirements for the LTO cycle and the noise assessment are presented in Table 1. ISA pressure and a deviation of 5 degrees from ISA temperature were assumed during the LTO cycle. The same flight conditions were applied for all engine designs.

Table 1. Key design parameters at top-of-climb and thrust requirements.

Altitude	10,668 m	$\eta_{poly,FAN}$	0.930	LTO Ratings (kN)		Noise Assessment Ratings (kN)	
Mach	0.78	$\eta_{poly,IPC}$	0.905	Take-off	143.1	Sideline	135.9
ISA	+10 K	$\eta_{poly,HPC}$	0.918	Climb-out	121.6	Cutback	68.0
Net thrust	25 kN	$\eta_{poly,HPT}$	0.900	Approach	42.9	Approach	19.1
Mass flow	196 kg/s	$\eta_{poly,LPT}$	0.930	Idle	10.0		

Additionally, the amount of the cooling flow required for the high pressure turbine (HPT) is computed for a turbine blade temperature limit of 1200 K, based on the model described in [23]. To represent a state-of-the-art engine turbine cooling capability, a blade cooling effectiveness of 0.73 is reached. This is achieved with internal convection cooling, film cooling, and thermal barrier coating included in the modeled engine.

2.2. Aircraft and Trajectory Modeling

The aircraft model used for the present study is implemented in GESTPAN and has been described in [24]. The aircraft is considered as a body and defined based on the A321-200, a narrow-body twin-engine jet airliner with a maximum take-off weight of 93,000 kg. The key design information was derived from [25], and the geometry is assumed fixed throughout the analysis.

Trajectories are established by integrating the flight dynamic equations for the aircraft, including its mass (solving for 5 differential equations −2D trajectories in time):

$$\begin{aligned} F_x &= F_N \cos(\gamma + \alpha) - L \sin(\gamma) - D \cos(\gamma) \\ F_y &= F_N \sin(\gamma + \alpha) + L \cos(\gamma) - D \sin(\gamma) - mg \end{aligned} \tag{3}$$

where F_x and F_y represent net thrust to the cartesian coordinate directions, α is the angle of attack, γ the center of gravity motion, and L and D are the lift and drag, respectively. The trajectories computed are coupled directly to algebraic equations for the propulsion system resulting in a nonlinear differential algebraic system of typically around 15 equations. Having take-off, approach, and landing trajectories available together with aircraft and engine performance modeling allows for estimating noise emissions from semi-empirical noise source models coupled with noise propagation methods [12]. The computed trajectories, which are used for the noise calculations, together with the microphone positioning for each point, are presented in Figure 1. Regarding the Sideline point, illustrated in Figure 1b, the microphone is not placed on the centerline of the runway, but at a distance of 450 m from it. The same trajectories are implemented in all the studied scenarios.

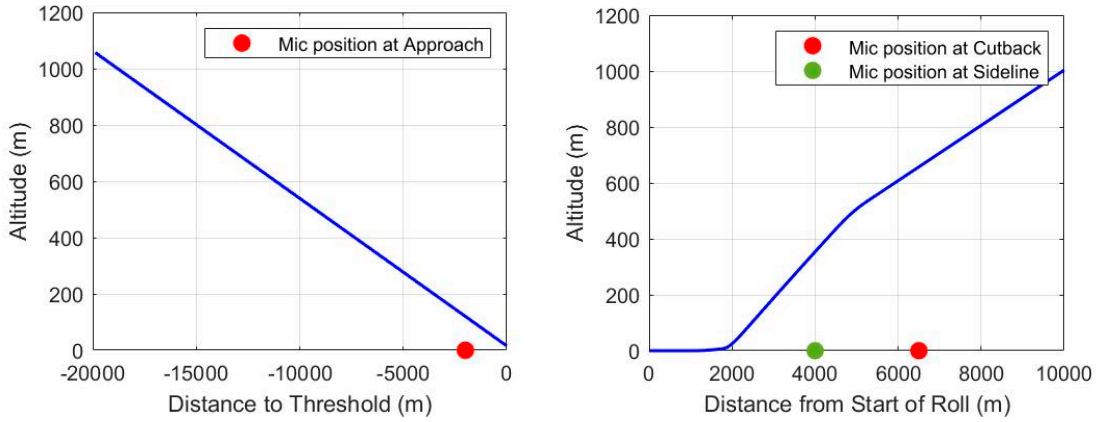

(**a**) (**b**)

Figure 1. Trajectories and microphone positioning for (**a**) approach and (**b**) cutback and sideline.

2.3. Noise Assessment Modeling

For the evaluation of noise, key performance data and trajectories from GESTPAN are inserted into the noise code CHOICE. CHOICE is a tool for the estimation of noise from engine and airframe components using semi-empirical source models [12]. The methods implemented in the noise estimation of each component are found in public literature. More specifically, noise produced from the fan and compressor inlet duct and fan discharge duct is computed using the method introduced by Heidmann [26]. According to this interim procedure, fan or compressor inlet duct

noise is analyzed to broadband, discrete tone, and combination tone noise, and fan discharge duct noise to broadband and discrete tone noise. The total noise is estimated as the summation of all the individual noise energy components. The combustor noise prediction method is based on the model described by Gliebe et al. [27]. This method is used for low emission combustor design using acoustic measurements of modern engines and it takes the combustor geometry, engine cycle conditions, directivity, and spectral frequency content into account. Turbine noise consists of broadband and discrete tone noise components which are related to the last stage relative tip velocity, the primary mass flow and local speed of sound at the turbine exit. The discrete tone noise is also dependent on the stator/rotor spacing. The model used for this component is based on the method described by Dunn and Peart [28]. Jet noise is modeled as presented by Russel [29]. This method can be used to estimate noise both from circular and coaxial jets, and it is based on extensive test data. The sound pressure levels from the test data are curve fitted, as a function of frequency and directivity, using bicubic splines and a third order Taylor series. The component noise levels are then defined for all frequencies and directivities. The airframe noise is estimated based on an empirical method presented by Golub et al. [30]. In this approach, model-scale and full-scale airframe noise measurements are used to identify the major noise sources and divide them into sub-components. The far-field is then derived by integrating the source map for each sub-region. Finally, the effective perceived noise level (EPNL) is calculated from the perceived noise level accounting for spectral irregularities and duration, as presented in the ICAO Noise Certification Workshop, [31].

2.4. NOx Assessment Modeling

Similar to noise emissions, CHEESE estimates NOx based on semi-empirical modeling methods found in public [8,32,33]. In this paper, a correlation developed by AECMA (European Association of Aerospace Industries) found in [33] and presented in Equation (4) below was adopted:

$$\text{EINOx} = 2.0 + 28.5\ \sqrt{(p_3/3100)}\ \exp((T_3 - 825)/250) \quad (4)$$

where p_3 and T_3 are the compressor outlet pressure and temperature in kPa and K, respectively, and EINOx is in g/kg. This correlation is said to provide a good estimation of the emissions of current large engines [33]. The optimal engines are evaluated according to the ICAO NOx certification procedures (LTO NOx).

2.5. Optimization and Trade Studies

A simplistic example of a 1D minimization problem is presented in Figure 2. In general, a necessary condition for the existence of a local extremum (local minimum or maximum) of a function that occurs within the interval where the function is differentiable is that it must be a stationary point. That means that the first derivative or gradient of the objective function at this point is zero, as illustrated in Figure 2. Thus, around an optimum point, there exists an interval where the objective function does not experience any or significant change. The intention is to quantify that region around the optimum point, which corresponds to the minimum installed SFC point (here ±0.5% in installed SFC), and examine trades between other variables, i.e., noise and NOx emissions.

The modeled engine is first optimized by varying the overall pressure ratio, fan pressure ratio, and bypass ratio. The optimization procedure establishes an engine with minimum installed SFC. The mission and aircraft geometry are considered fixed and the key design parameters, presented in Table 1, are kept constant, with the exception of the mass flow. The mechanical design of the engine and some key parameters, such as the mass flow and cooling flow, are directly dependent on the optimization variables and therefore vary during the procedure. The optimization procedure is carried out using an open-source framework introduced by Gray et al. [34]. It is a high-performance computing platform for multidisciplinary design optimization that uses Newton-type algorithms to solve coupled systems. Once the optimum point has been established, two study cases are examined.

The first refers to the variation of the OPR, by fixing FPR and BPR to their optimal values. Two points, close to the optimal, are then selected and noise and emissions are evaluated. Similarly, in the second case, the OPR is fixed, and variation in FPR and BPR is allowed to establish close to optimal cycles and examine trades with noise and emissions. A schematic representation of the described analysis is illustrated in Figure 3. The results demonstrated in the next section are plotted using either Python or MATLAB functions. The choice of which parameters to be presented from the engine cycle variation was based on their dependence on the optimization procedure or their effect on the noise and NOx emissions. Regarding the noise results, only the noise level from the components that contribute the most to the total noise level is depicted. Finally, NOx emissions for all the phases of the LTO cycle are presented, and the total NOx mass is calculated by multiplying the emission index of each phase with the corresponding duration.

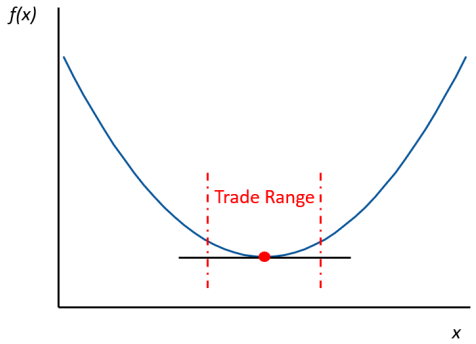

Figure 2. Graph of a given f(x), with a minimum and a trade range.

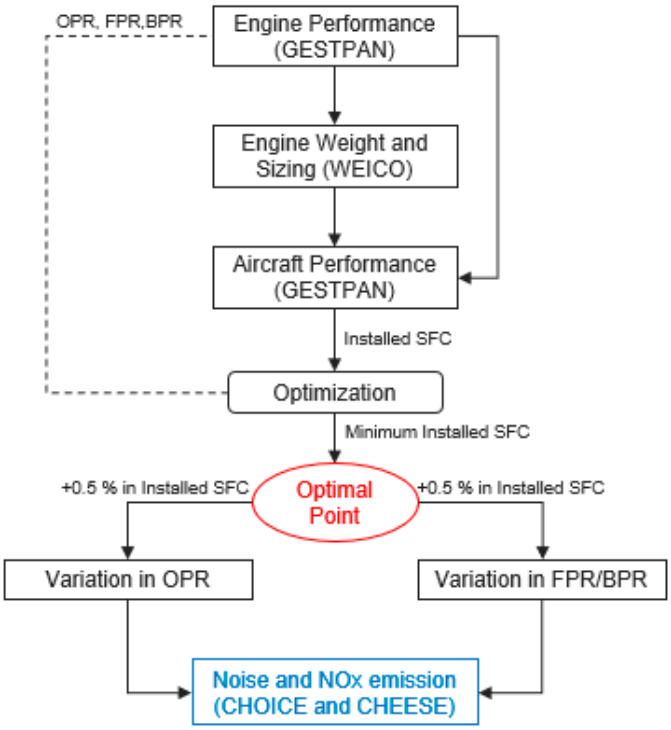

Figure 3. Flow chart of the research process.

3. Results

3.1. Tool Validation

For the thrust class and performance most relevant here, the Leap-1A family engines were selected as validation cases. Using component efficiency predictions as described in [21,22], cycles are established to match the public data found for Leap-1A26 and Leap-1A32. This includes the performance data, LTO cycle NOx data, and noise levels listed in the ICAO NOx data bank and noise fact sheet [19,20,35]. The LTO take-off ratings are 120.6 kN and 143.1 kN for Leap-1A26 and Leap-1A32, respectively, as defined in the ICAO emissions databank [20].

Table 2 contains the comparison between the models and the real engines. Regarding the performance and the mechanical design, it is observed that there is generally a good correlation between the simulated engine and the reported data. Public data found for the cruise BPR and SFC do not specify the corresponding variant of the Leap-1A and thus are not included in Table 2. The estimated engine weight from the model corresponds to the dry weight, which justifies the deviation from the one provided by the literature. The engine length from the public data accounts for the fan casing which is not included in the model. For the fuel flow, it is observed that, although there are small deviations, the trend of the values and the relative difference between the two simulated and the two real engines are similar.

Table 2. Simulated engine key data compared to real data.

		Leap-1A26			**Leap-1A32**		
		Public Data	**Model**	**Diff (%)**	**Public Data**	**Model**	**Diff (%)**
Cruise	BPR	NA	11.59	-	NA	11.59	-
	SFC (mg/Ns)	NA	14.53	-	NA	14.53	-
LTO take-off	OPR	33.3	33.71	1.2	38.6	39.24	1.7
	BPR	11.1	11.0	−0.9	10.5	10.6	1.0
Fan Diameter (m)		1.98	1.98	0.0	1.98	1.98	0.0
Bare Engine weight (kg)		2990 (with fluids)	2817	−5.8	2990 (with fluids)	2817	−5.8
Engine length (m)		3.328	3.102	−6.8	3.328	3.102	−6.8
Engine architecture		1 Fan – 3 IPC – 10 HPC – 2 HPT – 7 LPT					
Fuel flow (kg/s)	Take-off	0.861	0.837	−2.8	1.062	1.031	−2.9
	Climb-out	0.710	0.685	−3.5	0.869	0.846	−2.6
	Approach	0.244	0.239	−2.0	0.284	0.282	−0.7
	Idle	0.091	0.091	0.0	0.098	0.102	4.1
EINOx (gNOx/kgFuel)	Take-off	30.80	32.12	4.3	59.74	39.39	−34.1
	Climb-out	13.38	26.48	97.9	32.35	32.46	0.3
	Approach	8.75	10.00	14.3	9.95	11.26	13.2
	Idle	4.61	4.70	2.0	4.85	5.00	3.1
EPNL total (EPNdB)	Sideline	85.8	86.4	0.7	88.3	87.6	−0.8
	Cutback	81.2	84.2	3.7	83.3	86.5	3.8
	Approach	92.0	94.3	2.5	94.7	95.3	0.6

It is observed that the noise from the simulated engine is comparable with the reported measurements. Part of the deviations can be attributed to different trajectories and flight conditions between the simulated engine and the measured data. On the other hand, the predicted NOx at the climb-out point of Leap1-A26 and the take-off point of Leap-1A32 deviate from the ICAO data substantially, despite the fact that the simulated fuel flow is in good agreement. It is then observed that the Leap-1A engine has an atypical characteristic for the climb-out and take-off points NOx emissions. The ratio between the EINOx at the climb-out point and the take off point is around 0.5, whilst the other engines with similar thrust class have this number about 0.8. This characteristic is attributed to the novel GE combustor type (Twin Annular Premixing Swirler) TAPS II, which cannot be captured by

the semi-empirical models found in public literature. Nevertheless, the predicted NOx emissions trend is considered reasonable when comparing the models and the real engines' data.

3.2. Engine Cycle Design Space Exploration

First, a global optimum operating point is determined for minimum installed SFC, defined in Equation (1), by allowing a variation in OPR, FPR, and BPR. The optimum point is demonstrated in Table 3. Around the optimum, a trade range of 0.5% penalty in the installed SFC is chosen defining three points (the two end points and the optimum). The trade space for OPR variation is depicted in Figure 4. It is in line with elementary theory to expect that varying the OPR leads to a change in the number of stages of the turbomachines. This appears as discontinuities in the installed SFC curve in Figure 4. As the OPR increases, while fixing the fan pressure ratio (FPR) and the pressure ratio split between compressors, the stage count increase in the high pressure compressor (HPC) results in the small step increases in the installed SFC. On the other hand, the sudden decrease of installed SFC at an OPR close to 48 is because of a stage count reduction in the low pressure turbine (LPT). Fixed FPR and specific thrust give a lower bypass ratio (BPR) with an increasing OPR, hence a lower power requirement for the LPT and the reduction in LPT stage counts.

Table 3. Optimum cycle at top-of-climb.

OPR	T4 (TET, ISA+10)	FPR	BPR	Fan Diameter
48.5	1650 K	1.60	8.6	1.85 m (73 inch)

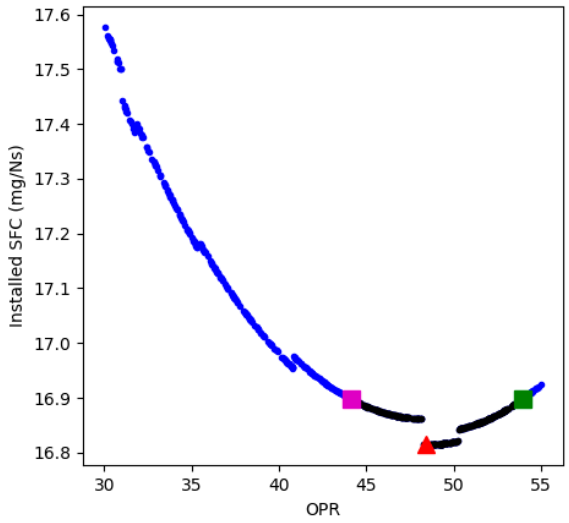

Figure 4. Cruise installed SFC as a function of OPR around the minimum.

The OPR optimum point, displayed by the red triangle in Figure 4, is found at an OPR of 48.5 at top-of-climb with an installed cruise SFC of 16.81 mg/Ns. The lower OPR point is located at 44.1 and the higher OPR point at 54.0. The key cruise parameters for the three points are presented in Table 4. Despite the relatively large variation in OPR, both the installed SFC and the uninstalled SFC experience modest change, whereas there are notable differences in the engine characteristics, i.e., number of stages and weight.

Table 4. Key data for the selected points in the OPR trade space. Numbers refer to cruise data unless otherwise stated.

OPR Trade Space	Low	Opt.	High
FPR	1.51	1.52	1.52
Inst. SFC (mg/Ns)	16.90	16.81	16.90
SFC (mg/Ns)	14.52	14.49	14.53
OPR	37.3	41.1	45.9
OPR (top-of-climb)	44.1	48.5	54.0
BPR	9.6	9.1	8.3
Mass flow (kg/s)	186.2	186.2	186.3
HPT cool. flow %	23.0	25.4	28.7
Nacelle drag [1] %	5.2	5.2	5.2
Mechanical Architecture			
HPC stages	11	11	12
LPT stages	7	6	6
Weight (kg)	4147	4050	4125

[1] Relative to net thrust.

The established optimal OPR point is used for the optimization of the low pressure system. Keeping the OPR constant while varying FPR and BPR, the resulting search space is reproduced in Figure 5. The cycle optimum is located close to an FPR of 1.60 at top-of-climb. The bypass ratio at this point is 8.6. The red triangle point represents the optimal point given in Table 3 above. As in the previous optimization case, a 0.5% variation in installed SFC is allowed. Thus, the lower FPR point results in a 77 inch fan, whereas the high FPR design has a 68 inch fan. The key cruise parameters for the three points are presented in Table 5. Similar to Figure 4, a lower level of discontinuity introduced by the stage counts change can be observed in Figure 5. The HPC stage increase from the 73 inch fan to the 68 inch fan is mainly due to a lower installation position of the HPC for a smaller fan design. This results from the same height ratio set for the inlet and outlet of the inter-compressor ducts. It is, however, a secondary effect compared to the weight change incurred by the change in fan size. Furthermore, although there is a relatively large variation in fan diameter and engine weight, the difference in installed SFC is minor. Mechanically, the optimal engine is a direct driven single stage fan with a three stage booster, an eleven stage high pressure compressor, a two stage high pressure turbine, and a six stage low pressure turbine.

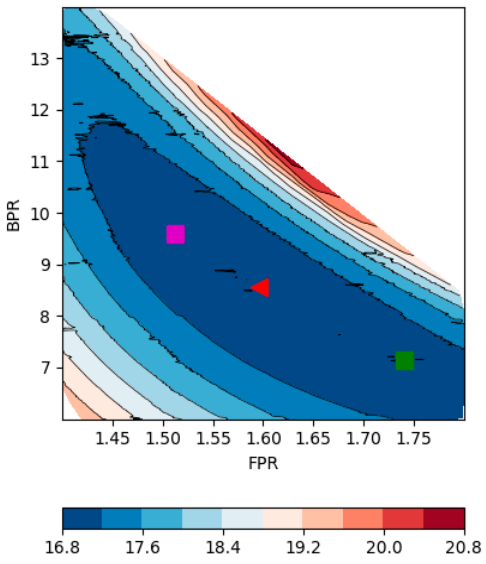

Figure 5. Cruise installed SFC contoured over top-of-climb FPR and BPR.

Table 5. Key data for the 77, 73, and 68 inch engine designs in the FPR/BPR trade space. Numbers refer to cruise data unless stated otherwise.

Fan Diameter (Inches)	**77**	**73**	**68**
FPR	1.44	1.52	1.64
FPR (top-of-climb)	1.51	1.60	1.74
Inst. SFC (mg/Ns)	16.90	16.81	16.90
SFC (mg/Ns)	14.41	14.49	14.73
OPR	41.3	41.1	40.9
BPR	10.1	9.1	7.6
BPR (top-of-climb)	9.6	8.6	7.1
Mass flow (kg/s)	206.4	186.2	160.1
Core jet velocity (m/s)	421.8	409.6	407.8
BP jet velocity (m/s)	306.7	308.9	312.4
Nacelle drag [1] %	5.6	5.2	4.7
Mechanical Architecture			
Fan Diameter (m)	1.95	1.85	1.73
HPC stages	11	11	12
LPT stages	6	6	6
Weight (kg)	4278	4050	3797
Fan rot. speed (rpm)	3979	4180	4493
LPT stage loading	2.98	2.97	2.96
LPT last stage tip vel. (m/s)	260.6	262.6	272.4

[1] Relative to net thrust.

3.3. Multidisciplinary Trades

In the previous section, two cases of engine cycle design space exploration were introduced, the low pressure system FPR/BPR space, and the core engine design space varying the OPR. Three points were selected for each case, corresponding to the cycle optimum and a 0.5% variation in installed SFC. For each point, the key performance parameters were presented, and the engine cycle performance was assessed. This section is dedicated to the evaluation of noise and NOx emissions for the chosen points.

Starting from the optimization of the OPR, Table 4, it is apparent that, despite the relatively large OPR variation, most of the key cruise parameters, including the installed SFC, remain almost constant. The corresponding results with regard to noise and NOx emissions are presented in Table 6, Table 7, and Figure 6.

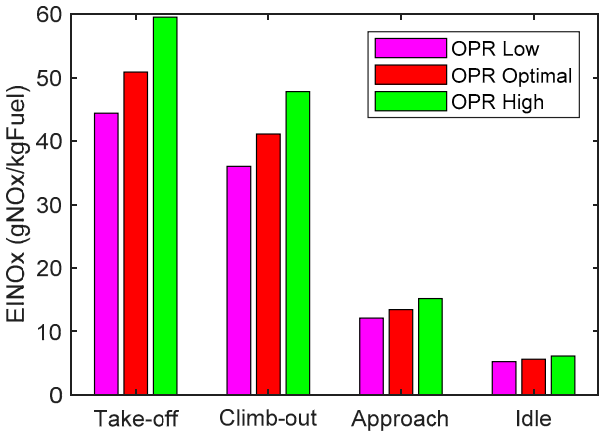

Figure 6. EINOx emissions for varying OPR cases at the LTO emission points.

Table 6. Noise source results in approach, sideline, and cutback for varying OPR cases.

		Low OPR	Optimal OPR	High OPR
Approach	Fan inlet	87.7	87.7	87.8
	Fan discharge	93.1	93.2	93.2
	LPT	82.0	81.8	82.5
	Engine	94.5	94.5	94.6
	Airframe	89.8	89.8	89.8
	Total	95.8	95.8	95.8
Cutback	Fan inlet	83.4	83.4	83.4
	Fan discharge	83.8	83.8	83.8
	LPT	72.8	72.7	73.5
	Jet	73.9	74.0	74.0
	Engine	87.0	87.0	87.0
	Total	87.1	87.1	87.1
Sideline	Fan inlet	72.2	72.2	72.2
	Fan discharge	79.2	79.2	79.2
	LPT	74.1	73.9	74.7
	Jet	84.4	84.5	84.7
	Engine	86.0	86.1	86.3
	Airframe	83.1	83.1	83.1
	Total	87.8	87.8	88.0
Cumulative EPNL		270.7	270.7	270.9

Table 7. Total LTO cycle NOx mass for varying OPR cases.

	NOx Mass (g)	Deviation
Low OPR	8028	−12%
Optimal OPR	9095	-
High OPR	10,589	16%

As can be observed, there is no significant effect on the total noise produced for the varying OPR cases. Since the optimization only influences the engine core of the propulsion system and the same trajectory is used for all cases, the airframe noise remains constant while the differences in total engine noise are essentially negligible. The trend, however, indicates that there is a slight increase in total noise with increasing OPR value, mainly driven by the LPT noise at approach and the LPT and jet noise at cutback and sideline. Even though the mentioned sources are not necessarily the driving noise factors, they are the ones experiencing largest variations.

On the contrary, the variation in NOx emissions is evident, especially in the Take-off and Climb-out points, where there is a deviation of about 15% between the three cases. There is an obvious trend of increasing emissions with increased OPR, which can easily be explained from the correlation presented in Equation (4). More specifically, increased OPR leads to increased compressor outlet temperature and pressure and therefore NOx emissions. The difference in the total LTO cycle NOx mass is also noteworthy, as can be seen from Table 7. For the lower OPR engine, a 12% decrease in total NOx mass can be traded for a roughly 0.5% increase in installed SFC.

Regarding the low pressure system optimization, Table 5, although the mass flow drops by 10–14% between the three cruise points and the FPR increases from 1.44 to 1.64; the installed SFC experiences minor variation over this relatively large design range. This indicates that the fuel burn trade is rather weak in this region and that the designer can choose the diameter within a relatively large range in the FPR/BPR space with a very modest fuel burn penalty. Thus, this should allow a relatively large design freedom with respect to noise, as the low pressure system is the major noise source for modern turbofans.

The main output from the semi-empirical noise and NOx emissions models are collected in Table 8, Table 9, and Figure 7. Regarding the NOx emissions, it is clear that the variation is notable between the three fan options. It is mainly the Take-off and Climb-out points that are indirectly influenced by the specific thrust of the three designs. The smaller engine has a higher FPR and, hence, a smaller thrust lapse. In other words, the thrust of the higher FPR engine does not go up as much as the lower FPR engines when running in take-off. Thus, it needs to throttle up and the resulting temperature in take-off remains somewhat higher than for the lower specific thrust configurations. In total, the LTO cycle NOx emissions' mass for the three engines is presented in Table 9. The relatively large difference in the total NOx mass is mainly driven by the fuel flow difference.

Table 8. Key noise drivers in approach, sideline, and cutback for the three engine designs.

		77 Inch Fan	73 Inch Fan	68 Inch Fan
Approach	Fan inlet	86.7	87.7	88.8
	Fan discharge	92.8	93.2	94.9
	LPT	81.3	81.8	82.4
	Engine	94.0	94.5	96.0
	Airframe	89.8	89.8	89.8
	Total	95.3	95.8	96.8
Cutback	Fan inlet	83.4	83.4	84.2
	Fan discharge	83.3	83.8	84.3
	LPT	72.3	72.7	73.5
	Jet	72.1	74.0	77.1
	Engine	86.7	87.0	87.8
	Total	86.7	87.1	87.8
Sideline	Fan inlet	71.3	72.2	75.4
	Fan discharge	78.6	79.2	80.1
	LPT	73.0	73.9	75.1
	Jet	82.6	84.5	87.7
	Engine	84.6	86.1	88.8
	Airframe	83.1	83.1	83.1
	Total	87.0	87.8	89.7
Cumulative EPNL		269.0	270.7	274.3

Table 9. Total LTO cycle NOx mass for 77/73/68 inch fan engines.

	NOx Mass (g)	Deviation
77 inch Fan	8483	−7%
73 inch Fan	9095	-
68 inch Fan	10,350	14%

Due to the parameter variation in FPR/BPR carried out here, only influencing the propulsion system, the airframe noise remains constant. Albeit, the total engine noise goes down with increasing BPR and decreasing FPR [7], as can be seen from Table 8. The relative importance of the fan inlet noise increases as expected at cutback while jet noise decreases significantly [7,36]. At the sideline, the jet becomes the dominant source of noise while fan inlet noise decreases. The fan discharge noise drops with decreasing FPR, reflecting the decrease in rotational speed as the diameter of the fan is increased (Table 5). The reduction in jet noise is driven by the fall in jet velocity in the fan stream. LPT noise rises with increasing FPR, despite the decrease in core mass flow. This trend is mainly driven by the increase in the tip velocity of the LPT's last stage (Table 5). In general, the trade between noise and engine performance is strongly dependent on the technology level assumed. For the state-of-the-art high BPR engines described in this paper, the rate of noise reduction is diminishing since the jet velocities and

jet noise are no longer so predominant. Except for the fan as still the major source of the total noise, the LPT becomes more important than ever [37].

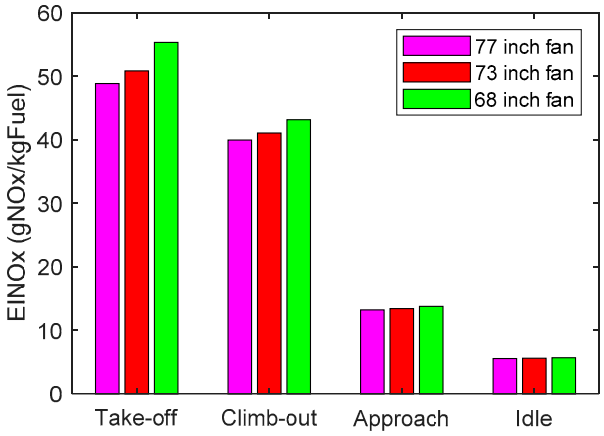

Figure 7. EINOx emissions for 77/73/68 inch fan engines at the LTO emission points.

A summary of the above multidisciplinary evaluation is shown in Table 10, where the key environmental trades are presented. It is noted that OPR can be traded for reduction in total LTO NOx mass with a minimum effect on fuel efficiency and noise emissions. On the other hand, variation in fan size allows for improvement in both NOx emissions and noise, with a slightly increased penalty in fuel efficiency.

Table 10. Environmental design trades.

OPR Design Space		**Low**	**Optimum**	**High**
Installed cruise SFC (mg/Ns)		16.90	16.81	16.90
Cruise fuel flow (kg/s)		0.338	0.336	0.338
LTO NOx Mass (g)		8028	9095	10,589
EPNL total	Approach	95.8	95.8	95.8
	Cutback	87.1	87.1	87.1
	Sideline	87.8	87.8	88.0
Cumulative EPNL		270.7	270.7	270.9
FPR/BPR Design Space		**77 Inches**	**73 Inches**	**68 Inches**
Installed cruise SFC (mg/Ns)		16.90	16.81	16.90
Cruise fuel flow (kg/s)		0.338	0.336	0.338
LTO NOx Mass (g)		8483	9095	10,350
EPNL total	Approach	95.3	95.8	96.8
	Cutback	86.7	87.1	87.8
	Sideline	87.0	87.8	89.7
Cumulative EPNL		269.0	270.7	274.3

4. Discussion

The OPR trade space SFC remains almost constant, as opposed to the FPR/BPR trade space where SFC varies with 2.2% across the three engine designs studied. Since the installed SFC accounts for the effect of engine weight and nacelle drag, this measure is expected to be a better metric for engine selection than pure SFC. The relevance of the installed SFC metric is supported by the fact that the optimal cycles predicted are quite realistic for a state-of-the-art turbofan engine of the given thrust class. Public data on BPR for the Leap-1A/Leap-1C engines are within the trade range predicted for the three engines. Thus, they are publicly stated diameters for these engines. If the pure SFC metric would

have been used, optimal BPR values larger than 12.0 are observed together with diameters outside the range of existing state-of-the-art engines for this thrust class.

After quantifying the range within which engine parameters can be traded a corresponding range in noise can be evaluated, ranging OPR does not have a significant effect on noise, and variations in fan diameter lead to an increase of up to 5.3 dB in cumulative noise from the 77 inch to the 68 inch fan. In the study presented by Gliebe and Janardan in [7], where noise emissions are evaluated for four engine designs with varying FPR and BPR, the fan diameter varies from 129.7 to 88.9 inches. The corresponding change in noise emissions is approximately 15 dB. When varying from the 129.7 to the 105.7 inch fan, a 4 dB increase in cumulative noise is observed. However, a 7 dB increase is observed from the 105.7 to the 96.3 inch fan, suggesting that the variation in noise level is not necessarily proportional to the variation in fan diameter. It should also be noted that, in the study by Gliebe and Janardan, different engine architecture was considered in some cases. For example, a geared fan was assumed for the lower FPR engines and a separate flow exhaust system for the largest engine. Compared with Cumpsty et al. [9], the 77 inch engine presented in this work is not optimized for noise, but the trend of going to larger fans is relatively flat in this region and only a modest further decrease in noise is expected. The slope in fuel burn penalty around the 77 inch fan is, however, relatively rapid indicating that it would require further fuel burn increase to reach the noise optimal point. Hence, the noise benefit would only be slightly larger than 1.7 dB for the noise optimal solution. This is well matched with the data that are predicted for the 2017 configuration [9], but a further knock on the current 0.5% SFC increase in fuel burn penalty would be expected. By also taking into account that the fuel burn trade would be larger than the SFC trade, it is not unreasonable to expect that we would approach the fuel burn penalty stated in [9].

When exploring the design space for OPR, a relatively large change in EINOx is observed corresponding to a 12% decrease in total NOx mass for the lower OPR engine with the same FPR of the optimal 73 inch fan engine. In the low pressure system optimization case, the improvement in NOx mass is lower, although still significant, amounts to a 7% reduction for the largest engine with the same OPR as the optimal.

Author Contributions: Conceptualization, T.G. and X.Z.; Methodology, E.M.T., T.G., and X.Z.; Software, E.M.T. and X.Z.; Supervision, T.G. and X.Z.; Validation, X.Z.; Writing—original draft, E.M.T.; Writing—review and editing, T.G. and X.Z. All authors have read and agreed to the published version of the manuscript.

Funding: We acknowledge gratefully the Swedish Transport Administration (TRV 2019/95826) for the funding and support of this work.

Conflicts of Interest: The authors declare no conflict of interest.

Nomenclature

α	Angle of attack	HPC	High pressure compressor
γ	Flight path angle	HPT	High pressure turbine
b	Fuel flow	IPC	Intermediate pressure compressor
A_{max}	Maximum nacelle area	ISA	International standard atmosphere
BPR	Bypass ratio	L	Lift
C_{d_nac}	Nacelle drag coefficient	LPT	Low pressure turbine
D	Drag	LTO	Landing and take-off cycle
$D_{engine\ mass}$	Drag due to the engine weight	m	Aircraft mass
$D_{nacelle}$	Nacelle drag	OPR	Overall pressure ratio
EINOx	Emission index of NOx	p_3	Compressor outlet pressure
F_N	Net thrust for all engines	q	Dynamic pressure
FPR	Fan pressure ratio	SFC	Specific fuel consumption
F_x	Net thrust horizontal component	$SFC_{installed}$	SFC accounting for installation effects
F_y	Net thrust vertical component	T_3	Compressor outlet temperature
g	Gravitational acceleration		

References

1. Peeters, P.M.; Middel, J.; Hoolhorst, A. *Fuel Efficiency of Commercial Aircraft: An Overview of Historical and Future Trends*; NLR-CR-2005-669; Netherlands National Aerospace Laboratory (NLR): Amsterdam, The Netherlands, 2005.
2. Correia, A.W.; Peters, J.L.; Levy, J.I.; Melly, S. *Residential Exposure to Aircraft Noise and Hospital Admissions for Cardiovascular Diseases: Multi-Airport Retrospective Study*; BMJ: Beijing, China, 2013; Volume 347.
3. Sparrow, V.; Gjestland, T.; Guski, R.; Richard, I.; Basner, M.; Hansell, A.; de Kluizenaar, Y.; Clark, C.; Janssen, S.; Mestre, V.; et al. *Aviation Noise Impacts White Paper*; ICAO: Montreal, QC, Canada, 2019; pp. 44–61.
4. Reduction of Noise at Source. Available online: https://www.icao.int/environmental-protection/pages/reduction-of-noise-at-source.aspx (accessed on 27 July 2020).
5. Zhang, M.; Filippone, A.; Bojdo, N. Multi-Objective Optimisation of Aircraft Departure Trajectories. *Aerosp. Sci. Technol.* **2018**, *79*, 37–47. [CrossRef]
6. Antoine, N.E.; Kroo, I.M. Aircraft Optimization for Minimal Environmental Impact. *J. Aircr.* **2004**, *41*, 790–797. [CrossRef]
7. Gliebe, P.R.; Janardan, B.A. *Ultra-High Bypass Engine Aeroacoustic Study*; General Electric Aircraft Engines: Cincinnati, OH, USA, 2003.
8. Kyprianidis, K.G.; Dahlquist, E. On the Trade-off between Aviation NOx and Energy Efficiency. *Appl. Energy* **2017**, *185*, 1506–1516. [CrossRef]
9. Cumpsty, N.; Mavris, D.; Kirby, M. *Aviation and the Environment: Outlook*; ICAO: Montreal, QC, Canada, 2019; pp. 24–38.
10. Grönstedt, T. Development of Methods for Analysis and Optimization of Complex Jet Engine Systems. Ph.D. Thesis, Chalmers University of Technology, Gothenburg, Sweden, 2000.
11. Grönstedt, T.; Au, D.; Kyprianidis, K.G.; Ogaji, S. Low-Pressure System Component Advancements and Its Influence on Future Turbofan Engine Emissions. In Proceedings of the ASME Turbo Expo 2009: Power for Land, Sea and Air, Orlando, FL, USA, 8–12 June 2009. [CrossRef]
12. Ellbrant, L.; Karlson, D. A Noise Prediction Tool for Subsonic Aircraft and Engines Including a Numerical Investigation of Noise Radiation. Master's Thesis, Chalmers University of Technology, Gothenburg, Sweden, 2008.
13. Grönstedt, T.; Irannezhad, M.; Lei, X.; Thulin, O.; Lundbladh, A. First and Second Law Analysis of Future Aircraft Engines. *J. Eng. Gas Turbines Power* **2014**, *136*. [CrossRef]
14. Grönstedt, T.; Wallin, M. A Comparative Study of Genetic Algorithms and Gradient Methods for RM12 Turbofan Engine Diagnostics and Performance Estimation. In Proceedings of the ASME Turbo Expo 2004: Power for Land, Sea and Air, Vienna, Austria, 14–17 June 2004; GT2004-53591. pp. 615–624.
15. Korsia, J.-J.; Spiegeleer, G.D. VITAL, an European R&D Program for Greener Aero-Engines. In Proceedings of the 25th International Congress of Aeronautical Sciences, Hamburg, Germany, 3–8 September 2006. ICAS 2006-5.6.1.
16. Wilfert, G.; Sieber, J.; Rolt, A.; Baker, N.; Touyeras, A.; Colantuoni, S. New Environmental Friendly Aero Engine Core Concepts. In Proceedings of the 18th International symposium on air breathing engines (IASBE), Beijing, China, 2–7 September 2007. ISABE – 2007 – 1120.
17. ESDU. *Drag of Axisymmetric Cowls at Zero Incidence for Subsonic Mach Numbers*; ESDU International: London, UK, 1981.
18. Robinson, M.; MacManus, D.G.; Sheaf, C. Aspects of Aero-Engine Nacelle Drag. *Proc. Inst. Mech. Eng. Part G J. Aerosp. Eng.* **2018**, *233*, 1667–1682. [CrossRef]
19. LEAP Overview CFM International. Available online: https://www.cfmaeroengines.com/wp-content/uploads/2017/09/Brochure_LEAPfiches_2017.pdf (accessed on 13 September 2020).
20. ICAO Aircraft Engine Emissions Databank. Available online: https://www.easa.europa.eu/domains/environment/icao-aircraft-engine-emissions-databank (accessed on 18 September 2020).
21. Grieb, H. *Projektierung von Turboflugtriebwerken*, 1st ed.; Birkhäuser: Basel, Switzerland, 2004.
22. Samuelsson, S.; Kyprianidis, K.G.; Grönstedt, T. Consistent Conceptual Design and Performance Modelling of Aero Engines. In Proceedings of the ASME Turbo Expo 2015: Turbine Technical Conference and Exposition, Montreal, QC, Canada, 15–19 June 2015. [CrossRef]

23. Wilcock, R.C.; Young, J.B.; Horlock, J.H. The Effect of Turbine Blade Cooling on the Cycle Efficiency of Gas Turbine Power Cycles. *J. Eng. Gas Turbines Power* **2005**, *127*, 109–120. [CrossRef]
24. Avellan, R.; Grönstedt, T. Preliminary Design of Subsonic Transport Aircraft/Engines. In Proceedings of the 18th International symposium on air breathing engines (IASBE), Beijing, China, 2–7 September 2007. ISABE 2007-1195.
25. Jenkinson, J.; Simpkin, P.; Rhodes, D. Civil Jet Aircraft Design. Available online: https://booksite.elsevier.com/9780340741528/appendices/data-a/table-1/table.htm (accessed on 3 October 2020).
26. Heidmann, M.F. *Interim Prediction Method for Fan and Compressor Source Noise*; NASA: Lewis Research Center: Cleveland, OH, USA, 1975.
27. Gliebe, P.; Mani, R.; Shin, H.; Mitchell, B.; Ashford, G.; Salamah, S.; Connell, S. *Aeroacoustic Prediction Codes*; NASA: Glenn Research Center: Cleveland, OH, USA, 2000.
28. Dunn, D.G.; Peart, N.A. *Aircraft Noise Source and Contour Estimation*; NASA: Boeing Commercial Airplane Co.: Seattle, WA, USA, 1973.
29. Russel, J.W. *An Empirical Method for Predicting the Mixing Noise Levels of Subsonic Circular and Coaxial Jets*; NASA: Langley Research Center: Hampton, VA, USA, 1984.
30. Golub, R.A.; Sen, R.; Hardy, B.; Yamamoto, K.; Guo, Y.-P.; Miller, G. *Airframe Noise Sub-Component Definition and Model*; NASA: Langley Research Center: Hampton, VA, USA, 2004.
31. Depitre, A. *Noise Certification Workshop, Session 2*; ICAO: Montreal, QC, Canada, 2006.
32. Chandrasekaran, N.; Guha, A. Study of Prediction Methods for NOx Emission from Turbofan Engines. *J. Propuls. Power* **2012**, *28*, 170–180. [CrossRef]
33. Green, J.E. Greener by Design—The Technology Challenge. *Aeronaut. J.* **2002**, *106*, 57–113. [CrossRef]
34. Gray, J.S.; Hwang, J.T.; Martins, J.R.R.A.; Moore, K.T.; Naylor, B.A. OpenMDAO: An Open-Source Framework for Multidisciplinary Design, Analysis, and Optimization. *Struct. Multidiscip. Optim.* **2019**, *59*, 1075–1104. [CrossRef]
35. EASA Certification Noise Levels. Available online: https://www.easa.europa.eu/domains/environment/easa-certification-noise-levels (accessed on 18 September 2020).
36. Daroukh, M. Effects of Distortion on Modern Turbofan Tonal Noise. Ph.D. Thesis, Institut National Polytechnique de Toulouse, Toulouse, France, 2017.
37. Nesbitt, E. Towards a Quieter Low Pressure Turbine: Design Characteristics and Prediction Needs. *Int. J. Aeroacoust.* **2010**, *10*, 1–15. [CrossRef]